Experimental characterization of acoustic beaming from an elastic plate by coupled symmetric leaky Lamb modes

T. J. Graham [1,*] J. D. Smith,[2] A. P. Hibbins [1] J. R. Sambles,[1] and T. A. Starkey[1]

[1]*Electromagnetic and Acoustic Materials Group, Department of Physics and Astronomy, University of Exeter, Stocker Road, Exeter EX4 4QL, United Kingdom*

[2]*DSTL, Porton Down, Salisbury, Wiltshire SP4 0JQ, United Kingdom*

(Received 8 January 2021; revised 20 May 2021; accepted 21 June 2021; published 6 July 2021)

Designer mode dispersions with properties such as negative or zero group velocities have applications in tailored wave propagation and energy redistribution. The modes of elastic plates can readily exhibit such phenomena by virtue of their bulk elastic properties and thickness. Here, we investigate the symmetric leaky Lamb modes within a thin flat aluminum-alloy plate submerged in water using pulsed broadband ultrasound, and experimentally characterize acoustic beaming from the plate caused by resonant transmission, which is enhanced via intrinsic negative dispersion of energy within the plate. The beaming of acoustic power occurs within a narrow frequency band in transmission over the negative group velocity region of the first-order symmetric leaky Lamb mode. Experimental characterization utilizes Fourier analysis and measurements of transmitted fields in time and space to obtain the leaky Lamb modes dispersion, which agree well with the predictions of a numerical model. This model is then used to visualize the pressure field and confirm the nature of the energy flow inside the plate. The properties of the acoustic focusing depend on the plate thickness and elastic material parameters, and may be readily controlled for a range of applications. Such phenomena may be exploited in other areas, such as in the microwave domain where designer mode dispersions can be developed using metamaterial concepts.

DOI: 10.1103/PhysRevB.104.045105

I. INTRODUCTION

Lamb waves are a type of guided acoustic wave that propagate in elastic media constrained by parallel planes and were formally studied at the start of the 19th century by Lamb [1]. There are two distinct types, symmetric (S_n) and antisymmetric (A_n), classified by the symmetry of particle motion with respect to the midplane of the plate. The lowest-order modes S_0 and A_0, exist from zero frequency, while an infinite family of higher-order modes exist with cutoff frequencies that correspond to half-wavelength quantization of the displacement field in the plate thickness. These waves are highly dispersive and are strongly dependent on the elastic material properties and the wavelength-thickness ratio (λ/t) of the plate in which they propagate. In the short-wavelength limit, $\lambda \lesssim t$, Lamb waves display bulk wave behavior and disperse toward the characteristic phase and group velocities of the elastic bulk wave speeds, i.e., the longitudinal or transverse velocities of the solid. By contrast, in the long-wavelength limit, $\lambda > t$, Lamb waves can have complex wave dispersions due to the mixed character of particle motions allowed by the boundary conditions. One type of Lamb wave is the leaky Lamb wave, which occurs when the modes of these elastic solids can be coupled to propagating radiation in the fluid that bounds the elastic media.

The complex nature of the dispersion relations of Lamb, and leaky Lamb, modes on elastic plates has been studied due to some of the unusual behaviors exhibited; namely regions in the dispersion relation where modes have either negative or zero in-plane group velocity, with a positive in-plane phase velocity (or vice versa). These conditions in the dispersion relation are typically referred to as the zero group velocity (ZGV) point and the negative group velocity (NGV) region. Historically, these ZGV and NGV points were experimentally observed [2–5], with later studies more fully describing the nature of the mode behavior [6–9] and the conditions required to achieve it [6,10].

The ZGV/NGV phenomena has predominately been reported in the literature in the dispersion of the first-order symmetric Lamb mode, S_1, ($\lambda/2$ compressional resonance in the plate thickness, L), and is present due to its interaction with the second-order symmetric Lamb mode, S_2, ($\lambda = L$ shear resonance) in the plate. Prada *et al.* [10] present the conditions required to achieve such dispersion relations; namely two modes of the same symmetry family (both symmetric or antisymmetric) and different parity (e.g., S_1, S_2) may couple via nonorthogonal mechanical displacements if their cutoff frequencies are sufficiently close, defined by the plate Poisson's ratio, ν. We note that as a consequence, there are bands in frequency-wave-vector space in which ZGV/NGV behavior can exist for higher-order Lamb modes, however, these are not widely realized due to constraints in available material parameters, i.e., the shear and compressional wave velocities. However, the Poisson's ratio of many metals is close to that required for critical coupling between symmetric Lamb modes, and so ZGV/NGV behaviors are readily observed in metal plates [10].

*tg310@exeter.ac.uk

These dispersion properties can be tailored to achieve a number of interesting effects with simple plate geometries, without employing more complex structural or metamaterial concepts [11]; for instance in the recent literature, near perfect geometric focusing of Lamb modes has been reported by tailoring dispersion properties using plate thickness to create an elastic lens [12]. Mode conversion between forward and backward dispersing waves has also been shown, using the free edge of an elastic plate [13].

Due to their utility in practical engineering applications, such as nondestructive testing (NDT) and material characterization, the propagation of Lamb, and leaky Lamb, modes guided by elastic solids has been studied extensively [14], and a substantial literature spanning a number of decades has amassed. NDT techniques that rely on leaky modes, where there is significant coupling of elastic energy from the solid to propagating acoustic waves in the surrounding fluid is of great practical importance. The radiation of leaky Lamb modes has therefore been studied for fluid-loaded geometries [15] of arbitrary shape, but also as a means to sense through fluid-loaded elastic boundaries. For instance, Kauffmann *et al.* demonstrate a scheme to obtain the multimodal leaky Lamb mode dispersion on a plate, which is driven by the leaky Lamb modes of an adjacent plate as a route to perform NDT within sealed environments [16]. Their studies have also discussed the influence of leaky Lamb mode dispersion and its influence on the transmission of propagating acoustic waves through plates; Aanes and coworkers show that acoustic waves projected at an elastic plate can produce a beam of acoustic energy in transmission, an effect that is attributed to the NGV/ZGV mode, and the extend to which the source excites it [17].

Furthermore, Aanes *et al.* [18] show that the NGV mode affects the radiated acoustic waves whereby the beam pattern of fields is strongly directional over narrow frequency ranges. By comparing the results of finite aperture numerical models to a point acoustic measurement of the transmission through a steel plate, the authors show an apparent enhanced transmission at normal incidence, and a shift in the resonant frequency peak between plane-wave and finite models for Lamb modes excited at normal incident. This phenomenon has been further examined theoretically in terms of the energy flux and complex dispersion relation in the region of negative dispersion [19,20]. The models, based upon explicit integral and asymptotic methods, developed by Glushkov *et al.* describe the enhanced transmission of acoustic energy (shown in Ref. [18]) in terms of the energy flow being limited from flowing laterally in the plate by energy vortices [20]. To date, these aspects have not been characterized and discussed for a single elastic plate system with comprehensive measurements.

In this study, we experimentally characterize the beaming behavior of acoustic energy, for sound projected at a flat aluminum-alloy plate, caused by the NGV region that exists due to the coupling between the first- and second-order symmetric leaky Lamb modes. Using a wholly acoustic method, sound was projected at a plate and the transmitted field was probed as a function of space. Measured data quantifies the leaky Lamb mode dispersion, and images the resulting beam profiles. The experimental results are compared, with excellent agreement, to a computationally modeled system. Using the finite element method (FEM) model, the behavior of the modes inside the plate is portrayed and explained in the context of resonant transmission and backward energy transport in the plate over the region of NGV. This study provides a complete experimental picture of the beaming phenomena described in part in the literature to date.

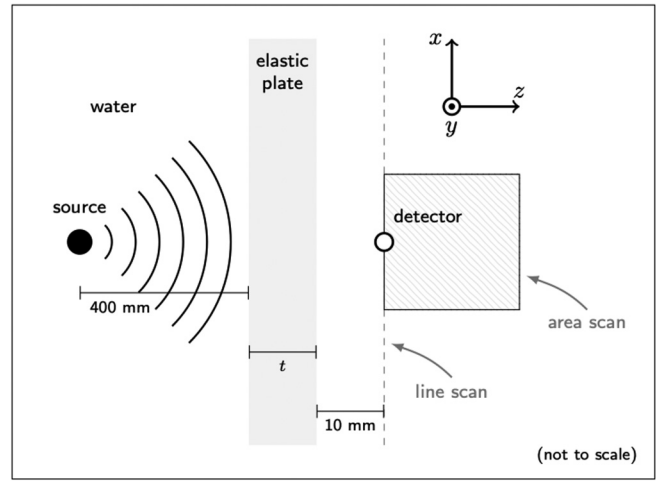

FIG. 1. Schematic diagram of the experimental arrangement of source, sample, and detector. Both source and sample remain fixed during scan measurements, whilst the detector is scanned in space to map the transmitted pressure field in the water.

II. EXPERIMENTAL AND MODELING METHODS

A. Ultrasonic characterization

All measurements were performed on a flat, square, aluminum-alloy (5083) plate, of thickness, $t = 9.8 \pm 0.1$ mm and area, $A = 605 \pm 1 \times 605 \pm 1$ mm, in a water tank with dimensions $3.0 \times 1.8 \times 1.2$ m (L×W×D), without wall or surface treatments. The sample was held in the water using a perspex frame (approximately 620 ± 1 mm by 740 ± 1 mm) so that the center of the plate was fixed at half the water depth and oriented with the plate normal parallel to the tank length. Before experiments, the plate was left to thermalize, and during measurements the water was static apart from small circulation associated with the detector movement.

The sample was excited using Hanning-windowed double-cycle ultrasonic pulses with center frequency 250 kHz projected using a ball-shaped Neptune-Sonar D70 transducer positioned 40.0 ± 0.5 cm from the plate surface. At this distance, the source excites over a range of incident angles, θ_i, with their associated range of in-plane wavevectors, $k_{\|}$ ($= k_0 \sin\theta_i$). Figure 1 shows a diagram of the experimental arrangement.

Ultrasound transmitted through the plate was detected with a Brüel & Kjær 8103 hydrophone placed 10.0 ± 0.1 mm from the sample surface. The detection hydrophone was scanned in space, using an *xyz* scanning stage (in-house built with Aerotech controllers) to map the acoustic propagation; the voltage, V, from the detector was recorded as a function of time, t, at each position in the scan. The x, y, and z coordinates correspond to vectors parallel to the width, W, depth, D, and length, L of the tank, respectively, so that xy maps a plane

parallel to the sample surface, and xz and yz map planes perpendicular to the sample surface.

Two scans of the transmitted pressure fields are performed; one line scan to extract the leaky Lamb mode dispersion, and an area scan to image the beaming effect. For these experiments the source was positioned on a line normal to the plate center to symmetrically excite the plate modes, and the detecting hydrophone surface was positioned 10.0 ± 0.1 mm from the plate. Line scan pressure field data was measured along a line from $x = -180$ mm to $+180$ mm, with resolution $\Delta x = 2.5$ mm, 10.0 ± 0.1 mm parallel to the plate surface, as indicated in the schematic in Fig. 1 (note any radial direction from the plate center would be equivalent). Area scan data was recorded over a 150×150 mm area beginning 10 mm from the plate surface in the xz plane with resolution $\Delta x = \Delta y = 2.5$ mm (see Fig. 1).

At each spatial point, signals are averaged in time over 250 repeat pulses to improve the signal-to-noise ratio. The data presented was sampled at sample rate $f_s = 9.62$ MHz, from when the pulse was triggered ($t = 0$) until maximum time $t_{\max} = 0.65$ ms. The resulting usable frequency range in these measurements is between 50 kHz and 500 kHz.

Using Fourier acoustic methods [21,22], the temporally and spatially dependent pressure field is used to extract the frequency, f, and in-plane wavevector, $k_{\|}$ (we consider k_x here), components of the transmitted fields. To remove artifacts that result from Fourier transforms, raw data were zero padded and windowed using a tapered-cosine window function [23,24]. The frequency resolution of the measurements is limited by the duration of signal recorded at each point $t_{\max}$. Likewise, the k-space resolution is limited by the scan length, $\Delta k = 1/x_{\max}$, and the k-space range is limited by the minimum scan step size, Δx (maximum wavevector $k_{\max} = 2\pi/\Delta x$).

B. Numerical simulations

To verify and explore the experimental results, a FEM model simulation of an idealized system was performed in COMSOL MULTIPHYSICS 5.4a. The model performed a frequency domain analysis: solving the full fluid-elastic interactions of a radially symmetric model plate, with a point source excitation. Responses were modeled from 200–500 kHz, and the transmitted complex acoustic pressure, p, was extracted.

To provide a realistic comparison to the experiment, the acoustic excitation was modeled by a point source positioned 400 mm away from the sample surface. The model sample has the same thickness as the experimental sample, and the aluminum alloy was assumed to have the following elastic properties, as measured or reported in the literature [25,26]: elastic modulus, $E = 72$ GPa, Poisson's ratio, $\sigma = 0.34$, and density, $\rho = 2660$ kg.m^{-3}.

III. RESULTS AND DISCUSSION

The method described above was used to excite and detect leaky Lamb modes in transmission to obtain their dispersion. The following sections present the measured time domain, frequency domain, and mode dispersion.

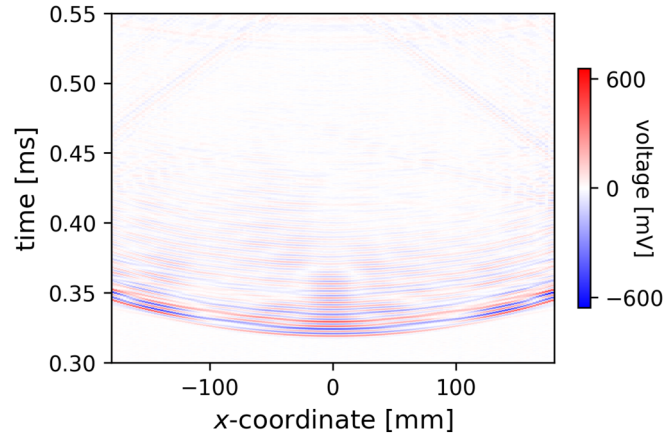

FIG. 2. Temporal signals detected for ultrasound transmitted through an aluminum-alloy plate. Acoustic pulses were measured along a line (from $x = -180$ mm to $+180$ mm, resolution $\Delta x = 2.5$ mm) 10.0 ± 0.1 mm parallel to the plate surface. The plate normal axis on which the source lies is at $x = 0$ mm.

A. Temporal measurements and frequency domain results

The measured temporal evolution of pulses transmitted through the plate sampled along a line 10 mm from, and parallel to, the sample surface is shown in Fig. 2. The leading edge of the pulse arrives first at the center of the scan area ($x = 0$), and arrives later at the detector as it moves further from the middle of the plate. The signal arriving at each point has experienced significant temporal dispersion having propagated through the plate. The figure also shows that some sound has been diffracted around the edges of the sample and is propagating across the face of the plate; this diffracted sound manifests as straight diagonal phase fronts appearing at the edges, $x = -180$ and $x = 180$ mm at $t = 0.47$ ms. The results also show that wavefronts contain some structure with signals concentrated at the center of the scan area, and at $x \approx \pm 135$ mm.

To further examine this signal concentration, the Fourier transform of the time signal, $\mathcal{F}(t)$, at each x coordinate is calculated to obtain the frequency domain signal (which is proportional to the pressure measured at the transducer). The Fourier transform is normalized in frequency to an equivalent scan without the sample present. The results shown in the top panel of Fig. 3 display a clear confinement of acoustic energy to a narrow spatial region over a small frequency band; the peak transmission amplitude in this region is ≈140%, confirming that the flat sample is generating some form of energy focusing effect of the transmitted fields. Below the high-intensity spot, there is also a horizontal band of intensity, and paraboliclike bands of low intensity moving up in frequency.

These experimental results are compared to the results of a numerical model of an idealized plate system. Figure 3 shows the comparison between experimental results (top) and modeled results (bottom). The model results show the normalized pressure field amplitude. There is good agreement; the model reproduces the concentration of power at $f \approx 300$ kHz and $x = 0$ mm, the horizontal band below it, and the dark bands with parabolalike shape with a minimum coinciding with the hot spot.

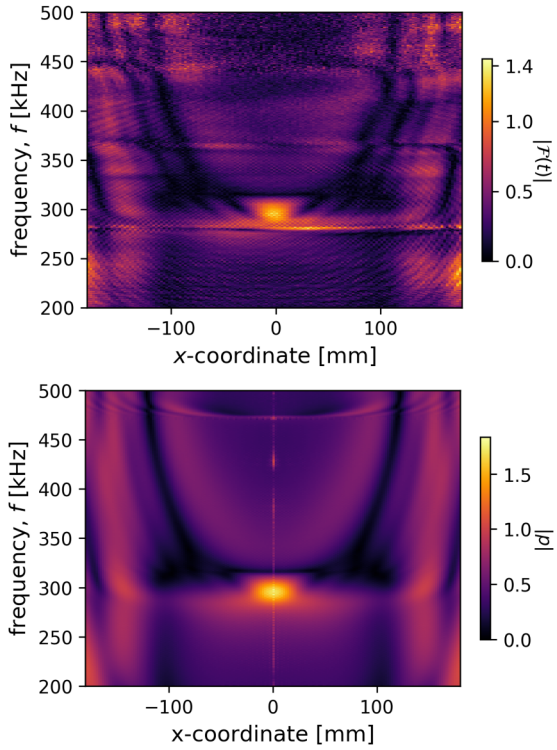

FIG. 3. Acoustic transmission through plate sample: Top plot shows the measured transmission calculated by the transmitted Fourier amplitude, $|\mathcal{F}(t)|$, normalized by an equivalent scan without the sample present. Bottom: numerical simulation results, presented as the normalized absolute pressure, $|p|$. In simulation data the line at $x = 0$ is an artefact of the model.

The model does not reproduce the low-intensity horizontal band at 280 kHz seen in the experimental data, since this is associated with the source-detector response functions. The contrast and width of features are slightly better defined in the model, something expected due to the model point source excitation, as opposed to the larger volume spherical source used in experiments.

B. Leaky Lamb mode dispersion

To obtain the mode dispersion from the experimental data, the spatial Fourier transform, $\mathcal{F}(x, t)$, of the frequency domain data is calculated; the results are shown in Fig. 4(a). From this measured data, it is clear that there are two modes that have cutoff frequencies in the region of 300–320 kHz, where apparent energy confinement was observed in Figs. 2 and 3.

Comparing the experimental momentum-space results to the predictions of an idealized FEM model [Fig. 4(b) bottom panel], and further comparing to the findings and subsequent conventions described in the literature [10], provides clarity; these modes are the first-order (S_1) and second-order (S_2) symmetric leaky Lamb modes, as labeled in the model data. At $k_x = 0$, the S_2 and S_{2b} (labeled following the convention set out by Prada *et al.* [10]) symmetric leaky Lamb modes are separated in frequency, at $f \approx 315$ kHz, by a low-intensity region; with increasing wavevector magnitude one mode dis-

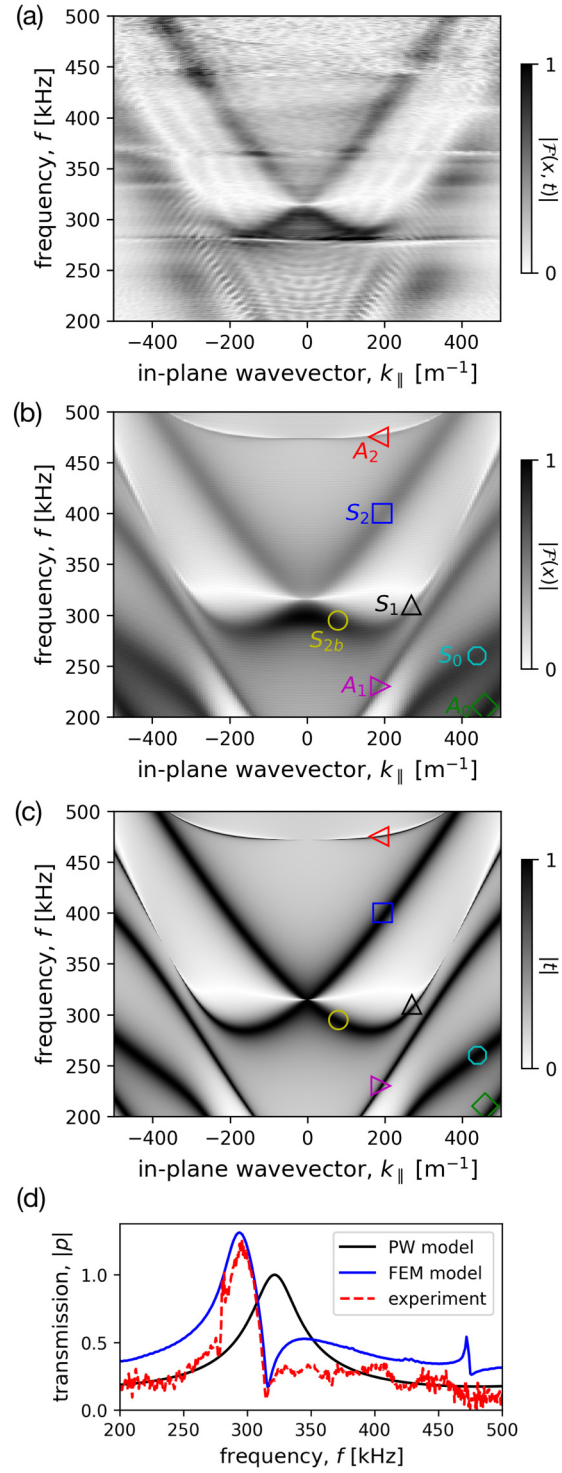

FIG. 4. Measured and modeled dispersion diagrams of leaky Lamb modes: (a) experimental results obtained through Fourier analysis of the pressure field line scan in transmission; (b) results of numerical simulation of an idealized experimental setup; and (c) results from an analytic plane-wave (PW) model [27]. The symmetric (S_n) and asymmetric (A_n) modes are indicated in (b) and (c), where the S_{2b} mode denotes the backward (negative) group velocity region caused by the coupling between the S_1 and S_2 symmetric modes. (d) compares the normal incidence transmission spectra obtained in (a)–(c).

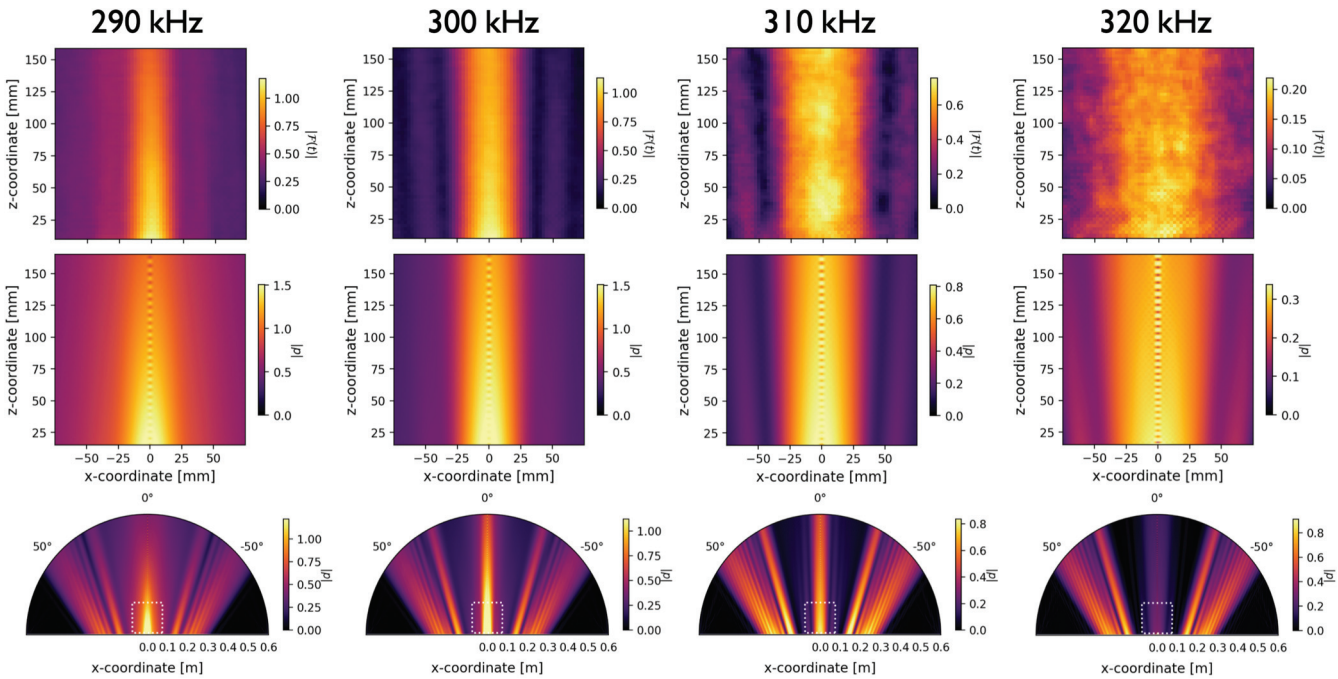

FIG. 5. XZ pressure maps for acoustic transmission in a 150 mm^2 area scanned on a plane normal to the sample surface at the plate center. Top: measured normalized spatial acoustic intensity maps. Middle: equivalent numerical (FEM) results for comparison. Bottom: larger area numerical evaluations of the transmitted pressure field (dotted square areas correspond to the scan area presented in top and middle field maps).

perses up in frequency and the other decreases in frequency through a region of negative dispersion when in-plane phase velocity (v_p) is negative for positive in-plane group velocity (v_g), before flattening to zero group velocity ($v_g = \nabla_k . f = 0$).

The measured mode dispersion shows good agreement with the FEM model for the S_1, S_2 and S_{2b} region of interest. In the experiment, the first-order antisymmetric, A_1, leaky Lamb mode is also weakly detected, however, due to limited scan length permitted by the experimental setup the Rayleigh S_0 and A_0 modes seen in the model at low frequency and large wavevector are not observed experimentally.

For completeness, we also compare the experiment and FEM model results to a plane-wave model. Figure 4(c) shows the mode dispersion as a function of $k_\parallel$, f, $|t|$, calculated following the approach of Anderson *et al.* [27] which accounts for the fluid-elastic solid interaction for a homogeneous flat plate without any internal damping. The plane-wave model broadly shows the same mode dispersion as the FEM model with three differences: (ii) the transmission peak that occurs at ≈300 kHz [Fig. 4(d)] are at slightly different frequencies and there is a low-intensity spectral feature at 315 kHz where the S_2/S_{2b} meet at $k_\parallel = 0$, which is absent for the plane-wave model; (ii) at normal incidence the transmission in the FEM model shows enhanced transmission (>1), whereas the plane-wave model peak intensity is 1; and (iii) the second-order antisymmetric mode, A_2 is excited at $k_\parallel = 0$ in the FEM model, but not in the plane-wave model. These differences are more obvious when comparing the normal incidence transmission (i.e., $k_\parallel = 0$) for the experiment, FEM model, and the plane-wave model, as shown in Fig. 4(d).

These differences between the plane-wave and FEM (point excitation) model arise due to the nature of the excitation pressure field presented to the elastic plate: a planar wavefront incident on the plate has a well-defined k vector across the plate, a curved wavefront, as in the experiment, presents a range of in-plane wavevectors across the plate surface, and consequently has a width in $\Delta k_\parallel$. The differences in peak location and an amplitude minimum are characteristic of panel measurements conducted with a curved incident wavefront where the transmission coefficient varies rapidly with angle (see the studies of Humphrey *et al.* for a full discussion [28,29]). The greater than unity transmission amplitude is due to the NGV region guiding power back toward the center of the plate, and thus being radiated to the surrounding fluid, as will be discovered in the following sections.

C. XZ transmission scan

To experimentally show how the energy is radiated from the plate and to verify the acoustic beaming effect in the far field reported by Aanes *et al.* [17], caused by the NGV region of the S_{2b} mode, we map the fields transmitted though the elastic plate. The transmitted pressure field is mapped on a two-dimensional (2D) plane normal to the plate surface in the x and z direction (as indicated in Fig. 1), and Fourier analyzed in time to obtain the pressure field.

Figure 5 compares the measured and numerical simulation results of the normalized pressure field transmitted through the aluminum plate at frequencies within the S_{2b} NGV band (f = 290, 300, and 300 kHz), and one frequency above (f = 320 kHz). Measured results are displayed as the normalized pressure amplitude relative to the pressure obtained at $x, z = 0$, 10 mm from the center of the plate when the plate is removed. Numerical results are presented in an equivalent way for comparison. There is excellent agreement between measured and modeled data for the area scan; both show

a well-confined collimated beam of power transmitted to the fluid by the plate; at the two lowest frequencies the normalized amplitude is greater than unity; at 310 kHz the beam is wider; at $f = 320$ kHz, now in the S_2 band, the transmitted pressure amplitude decreases significantly and the beam widens further.

Using the numerical model and evaluating the transmission over a wider area (see bottom panels in Fig. 5) it is clear that over the NGV region of the S_{2b} mode's dispersion the acoustic energy transmitted through the plate at normal incidence is relatively large, while for normal dispersion ($+v_p$ and $+v_g$) this beaming effect is not a prominent feature, and more energy is resonantly coupled through the plate at larger angles by the leaky Lamb modes that exist at higher wavevector.

Our results experimentally verify that energy transmitted by the plate has a spatial intensity profile reminiscent of a collimated beam due to the NGV region that occurs due to the S_1/S_2 coupling at low wave number as predicted by theoretical results presented by Aanes and coworkers [17,18] in earlier works.

We interpret this as a feature of the mode width in momentum space, as shown in Fig. 4; the S_{2b} mode has intensity over a broad wavevector range (Δk from -80 m^{-1} to 80 m^{-1}) for a single frequency; this means that there are a range of acceptance angles at which sound will undergo resonant transmission. This means that the plate behaves as a frequency-dependent aperture for sound and is diffraction limited in the normal way. This aperture effect occurs regardless of whether the leaky Lamb mode supported by the plate is undergoing normal or NGV dispersion—as seen by comparing data for the lowest and highest frequencies in Fig. 5—however, the nature of the dispersion does strongly influence transmission amplitudes as shown by comparing relative magnitudes.

D. FEM plate modes

To further explore the behavior of leaky Lamb modes, the time-averaged pressure field and power flow above, below, and within the aluminum-alloy plate are visualized, using the numerical model. The plate response is compared at two frequencies; $f = 300$ kHz, which lies in the NGV region and demonstrates strong acoustic beam effects; and above the NGV region where mode dispersion is normal at $f = 320$ kHz.

Figure 6 compares the pressure distributions at these frequencies, with the acoustic intensity vector overlaid. In these figures the point source is located at $(r, z) = (0, -405$ mm), the plate midpoint is at $(r, z) = (0, 0)$, and only positive radius values are shown (the model assumes axial symmetry around $r = 0$).

By examining the intensity and energy flow within the plate we can observe the group velocity behavior shown in the dispersion plots. As shown in Fig. 4, at 300 kHz, the S_{2b} mode has a relatively broad width with Fourier spectral intensity over a range of wavevectors from $k_{\|} = 0$ to $\approx 80\,\mathrm{m}^{-1}$, and, with increasing momentum, intersects S_1, A_1, and then S_0 and A_0 at much higher wave number. In Fig. 6(a), we see that over a range of incident angles (in-plane wavevectors) the power flow within the plate is moving toward the plate center, before being reradiated in transmission close to the plate center where there is a maximum in pressure. The range in real space from 0 to ≈ 90 mm where power flow transitions from backward flow to forward flow corresponds to the width of the S_{2b} mode in the dispersion plots. At greater distances along the plate (>125 mm), there is significant power transmitted to the fluid, which corresponds to those leaky modes with larger wavevectors.

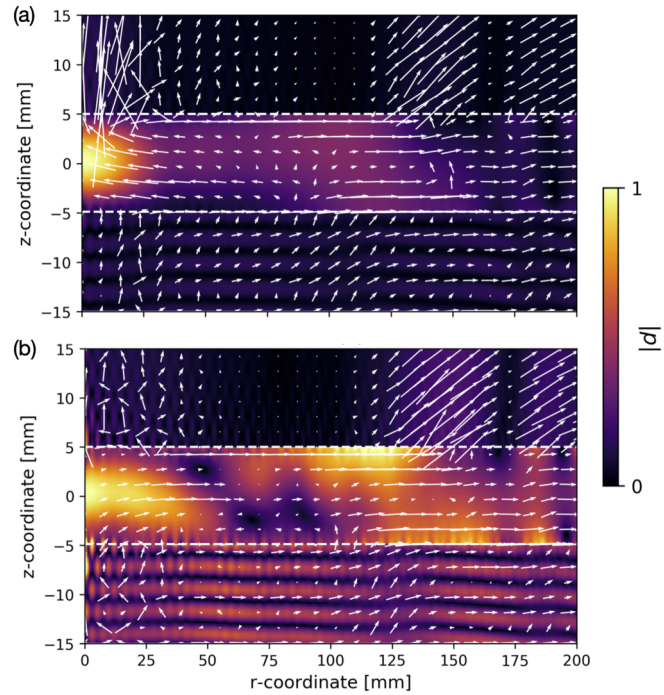

FIG. 6. Comparison of absolute pressure and acoustic intensity of plate response for (a) NGV mode dispersion ($f = 300$ kHz) and (b) normal mode dispersion ($f = 320$ kHz). The relative absolute pressure values are scaled to unity. Arrows indicate the acoustic intensity; vectors give direction, and magnitude is proportional to strength.

As a contrasting example, at 320 kHz, all modes on the plate have normal positive phase and group velocity dispersion behavior (Fig. 4). It is unsurprising therefore that when viewing the calculated power flow in Fig. 6(b) the mean power flow is along the plate away from the source, and there is no longer a high-intensity pressure spot at the plate center.

IV. CONCLUSIONS

The coupling between the S_1 and the S_2 symmetric leaky Lamb modes, causes a mode to disperse with phase and group velocity with opposite sign. Here experimentally, using an wholly acoustic field mapping technique, the mode dispersion was characterized and the acoustic beaming of energy from a plate in transmission was investigated. It was shown that the leaky Lamb modes of a flat, unstructured 9.8 ± 0.1 mm thick aluminum-alloy plate produce acoustic beaming when isonified by a transducer producing nonplanar wavefronts.

Field mapping measurements along a line, and Fourier analysis, were using to obtain the leaky mode dispersion in transmission as a function of frequency and in-plane wavevector. Area field maps were used to map the beaming effect.

Measured results were compared to an idealized finite element method model of the experimental setup with excellent agreement, and also confirmed theoretical results presented in the literature for similar plates with the same modal behavior. Model results were also used to explore the backward energy flow in the plate in the NGV region, to demonstrate why the normal incidence transmission may have an amplitude >1.

The acoustic beaming is associated with the first-order symmetric leaky Lamb mode, which exists over a relatively broad range of in-plane momenta close to $k = 0$ for a fixed frequency range. By virtue of this mode dispersion, incident sound undergoes resonant transmission over a range of input angles, giving the plate the appearance of an open aperture. The transmitted beam is highly collimated, and its intensity is further enhanced due to the mode having negative in-plane group velocity, which transports power towards the center of the plate. In essence, the plate is behaving as a closed frequency-dependent aperture for sound, which is further enhanced by the energy flow toward the plate center due to the NGV mode behavior.

The results presented here may be tailored to fit specific frequency ranges by simply changing the thickness of the plate or by selecting the elastic properties. Applications of such a phenomenon may be the control of acoustic energy for improved absorption or the directional transmission in an underwater environment. Further, this effect is not limited to acoustic applications and may be used for electromagnetic beam generation using tailored mode dispersions in planar electromagnetic metasurfaces.

All data created during this research are openly available from the University of Exeter's institutional repository [30].

ACKNOWLEDGMENTS

We acknowledge financial support from the Engineering and Physical Sciences Research Council (EPSRC) of the United Kingdom, via the EPSRC Centre for Doctoral Training in Metamaterials (Grant No. EP/L015331/1), and Thales UK through an Industrial CASE Training Account (voucher number 14440030). T.A.S. acknowledges financial support from DSTL.

APPENDIX: PLANE-WAVE MODEL

The model transmission data presented in Figs. 4(c) and 4(d) was calculated following the approach by Anderson *et al.* [27]. The model assumes fluid-elastic solid interaction for a homogeneous flat plate without internal damping. Transmission was calculated as a function of in-plane wavevector, $k_\parallel$, and frequency, f, to image the mode dispersion [Fig. 4(c)] and transmission [Fig. 4(d)] for a normal incident plane wave.

The transmission coefficient is given by

$$T = \frac{iY(A+S)}{(A+iY)(S-iY)} \tag{A1}$$

where Y, A, and S are

$$Y = (\rho_f/\rho_p)\left(k_t^4\right)\kappa_l/\kappa_f \tag{A2}$$

$$A = \left(k_t^2 - 2k_\parallel^2\right)^2 \tan(\kappa_l d/2) + 4k_\parallel^2\kappa_t\kappa_l \tan(\kappa_t d/2) \tag{A3}$$

$$S = \left(k_t^2 - 2k_\parallel^2\right)^2 \cot(\kappa_l d/2) + 4k_\parallel^2\kappa_t\kappa_l \cot(\kappa_t d/2), \tag{A4}$$

where $\kappa_f = \sqrt{k_f^2}$, $\kappa_l = \sqrt{k_l^2 - k_\parallel^2}$, and $\kappa_t = \sqrt{k_t^2 - k_\parallel^2}$. The wave numbers for longitudinal, transverse modes in the plate and in the fluid are given by $k_f = 2\pi f/c_f$, $k_l = 2\pi f/c_l$, $k_t = 2\pi f/c_t$, as defined by their respective velocities of sound. Parameters used were; velocities $c_f = 1490\ \mathrm{ms}^{-1}$, $c_l = 6248\ \mathrm{ms}^{-1}$, $c_t = 3147\ \mathrm{ms}^{-1}$; plate thickness $d = 10$ mm; fluid and plate densities $\rho_f = 997\ \mathrm{kg.m}^{-3}$ and $\rho_p = 2665\ \mathrm{kg.m}^{-3}$.

[1] H. Lamb, On waves in an elastic plate, Proc. R. Soc. Lond. A **93**, 114 (1917).
[2] I. Tolstoy and E. Usdin, Wave propagation in elastic Plates: Low and high mode dispersion, J. Acoust. Soc. Am. **29**, 37 (1957).
[3] A. H. Meitzler, Backward-wave transmission of stress pulses in elastic cylinders and plates, J. Acoust. Soc. Am. **38**, 835 (1965).
[4] R. L. Weaver and P. Yih-Hsing, Spectra of transient waves in elastic plates, J. Acoust. Soc. Am. **72**, 1933 (1982).
[5] J. Wolf, T. D. K. Ngoc, R. Kille, and W. G. Mayer, Investigation of Lamb waves having a negative group velocity, J. Acoust. Soc. Am. **83**, 122 (1988).
[6] M. F. Werby and H. Uberall, The analysis and interpretation of some special properties of higher order symmetric Lamb waves: The case for plates, J. Acoust. Soc. Am. **111**, 2686 (2002).
[7] F. Simonetti and M. J. S. Lowe, On the meaning of Lamb mode nonpropagating branches, J. Acoust. Soc. Am. **118**, 186 (2005).
[8] C. Prada, O. Balogun, and T. W. Murray, Laser-based ultrasonic generation and detection of zero-group velocity Lamb waves in thin plates, Appl. Phys. Lett. **87**, 194109 (2005).
[9] C. Prada, D. Clorennec, and D. Royer, Power law decay of zero group velocity Lamb modes, Wave Motion **45**, 723 (2008).
[10] C. Prada, D. Clorennec, and D. Royer, Local vibration of an elastic plate and zero-group velocity Lamb modes, J. Acoust. Soc. Am. **124**, 203 (2008).
[11] R. V. Craster and S. Guenneau, *Acoustic Metamaterials: Negative Refraction, Imaging, Lensing and Cloaking* (Springer, Berlin, 2012).
[12] F. D. Philippe, T. W. Murray, and C. Prada, Focusing on plates: Controlling guided waves using negative refraction, Sci. Rep. **5**, 11112 (2015).
[13] B. Gérardin, J. Laurent, C. Prada, and A. Aubry, Negative reflection of Lamb waves at a free edge: Tunable focusing and mimicking phase conjugation, J. Acoust. Soc. Am. **140**, 591 (2016).
[14] I. A. Viktorov, *Rayleigh and Lamb Waves*, 1st ed. (Springer, New York, 1967).

[15] M. Mazzotti, A. Marzani, and I. Bartoli, Dispersion analysis of leaky guided waves in fluid-loaded waveguides of generic shape, Ultrasonics **54**, 408 (2014).

[16] P. Kauffmann, M.-A. Ploix, J.-F. Chaix, C. Potel, C. Gueudre, G. Corneloup, and F. Baque, Multi-modal leaky Lamb waves in two parallel and immersed plates: Theoretical considerations, simulations, and measurements, J. Acoust. Soc. Am. **145**, 1018 (2019).

[17] M. Aanes, K. D. Lohne, P. Lunde, and M. Vestrheim, Finite aperture influence on energy concentration, frequency shift, and signal enhancement, for acoustic transmission in the negative group velocity region of the S_1 leaky Lamb mode, in *2016 IEEE Int. Ultrason. Symp.* (2016), pp. 1–4.

[18] M. Aanes, K. D. Lohne, P. Lunde, and M. Vestrheim, Beam diffraction effects in sound transmission of a fluid-embedded viscoelastic plate at normal incidence, J. Acoust. Soc. Am. **140**, EL67 (2016).

[19] I. A. Nedospasov, V. G. Mozhaev, and I. E. Kuznetsova, Unusual energy properties of leaky backward Lamb waves in a submerged plate, Ultrasonics **77**, 95 (2017).

[20] E. V. Glushkov, N. V. Glushkova, and O. A. Miakisheva, Backward waves and energy fluxes excited in acoustic medium with an immersed plate, Ultrasonics **94**, 158 (2019).

[21] D. Alleyne and P. Cawley, A two-dimensional Fourier transform method for the measurement of propagating multimode signals, J. Acoust. Soc. Am. **89**, 1159 (1991).

[22] T. J. Graham, A. P. Hibbins, J. R. Sambles, and T. A. Starkey, Underwater acoustic surface waves on a periodically perforated metal plate, J. Acoust. Soc. Am. **146**, 4569 (2019).

[23] P. Podder, T. Z. Khan, M. H. Khan, and M. M. Rahman, Comparative performance analysis of hamming, hanning and blackman window, Int. J. Comput. Appl. **96**, 975 (2014).

[24] R. Hovden, Y. Jiang, H. L. Xin, and L. F. Kourkoutis, Periodic artifact reduction in Fourier transforms of full field atomic resolution images, Microsc. Microanal. **21**, 436 (2014).

[25] J. M. Holt, C. Gibson, and C. Y. Ho, *Structural Alloys Handbook*, Vol. 1 (Purdue University, Indiana, 1996).

[26] M. J. Holmes, N. G. Parker, and M. J. W. Povey, Temperature dependence of bulk viscosity in water using acoustic spectroscopy, J. Phys.: Conf. Ser. **269**, 012011 (2011).

[27] M. J. Anderson, P. R. Martin, and C. M. Fortunko, Resonant transmission of a 3-dimensional acoustic sound beam through a solid plate in air—theory and measurement, J. Acoust. Soc. Am. **98**, 2628 (1995).

[28] V. F. Humphrey and H. O. Berktay, The transmission coefficient of a panel measured with a parametric source, J. Sound Vib. **101**, 85 (1985).

[29] V. F. Humphrey and J. Smith, Panel transmission measurements: The influence of the non plane wave nature of the incident field, J. Acoust. Soc. Am. **123**, 3591 (2008).

[30] https://ore.exeter.ac.uk/repository/.